# Improved visual acuity using a retinal implant and an optimized stimulation strategy

To cite this article before publication: Wei Tong *et al* 2019 *J. Neural Eng.* in press https://doi.org/10.1088/1741-2552/ab5299

**IOP** Publishing Journal Title
Journal **XX** (XXXX) XXXXXX https://doi.org/XXXX/XXXX

# Improved visual acuity using a retinal implant and an optimized stimulation strategy

**Wei Tong[1,2,3], Melanie Stamp[2], Nicholas V. Apollo[2,4], Kumaravelu Ganesan[2], Hamish Meffin[1,3], Steven Prawer[2], David J. Garrett[2], Michael R. Ibbotson[1,3,*]**

[1] National Vision Research Institute, Australian College of Optometry, Australia
[2] School of Physics, The University of Melbourne, Australia
[3] Department of Optometry and Vision Sciences, The University of Melbourne, Australia
[4] Center for Neural Engineering and Therapeutics, University of Pennsylvania, Philadelphia, USA

* E-mail: mibbotson@nvri.org.au

Received xxxxxx
Accepted for publication xxxxxx
Published xxxxxx

## Abstract

*Objective.* Retinal prosthetic devices hold great promise for the treatment of retinal degenerative diseases such as retinitis pigmentosa and age-related macular degeneration. Through electrical stimulation of the surviving retinal neurons, these devices evoke visual signals that are then relayed to the brain. Currently, the visual prostheses used in clinical trials have few electrodes, thus limiting visual acuity. Electrode arrays with high electrode densities have been developed using novel technologies, including diamond growth and laser machining, and these may provide a more promising route to achieve high visual acuity in blind patients. *Approach.* Here, we studied the potential spatial resolution of electrical stimulation using diamond electrodes. We did this by labeling retinal ganglion cells in whole mount retina with a calcium indicator in wild-type rats and those with retinal degeneration. We imaged the ganglion cell responses to a range of stimulation parameters, including pulse duration and return electrode configuration. *Main results.* With sub-retinal stimulation, in which electrodes were in contact with the intact or degenerated photoreceptor layer, we found that biphasic pulses of 0.1 ms phase duration and a local return configuration was the most effective in confining the retinal ganglion cell activation patterns, while also remaining within the safety limits of the materials and providing the best power efficiency. *Significance.* These results provide an optimized stimulation strategy for retinal implants, which if implemented in a retinal prosthetic is expected to improve the achievable visual acuity.

Keywords: retinal prosthesis, stimulation strategy, diamond electrode array

## 1. Introduction

Blindness has a significant impact on an individual's quality of life and severe socioeconomic ramifications. Retinal diseases are a leading cause of vision loss (1), and in some developed countries they are responsible for more than half of the cases of blindness (2). In some types of retinal diseases, such as retinitis pigmentosa (RP) and age-related macular degeneration (AMD), the light sensitive cells (photoreceptors) are lost and, thus, the ability to transduce light into useful visual signals (3). One potential treatment for these diseases is to implant microelectronic retinal prostheses, which are designed to electrically stimulate the surviving retinal neurons, including bipolar cells and ganglion cells. Signals from the latter send information to the brain via the optic nerve where they are interpreted as images (3).



 

Recent years have witnessed significant advances in the development of retinal implants. Several devices, including Second Sight's Argus II (4), Retina Implant AG's Alpha IMS (5), and Bionic Vision Australia's suprachoroidal devices (6) have been implanted into human patients, which have restored a limited sense of vision. In spite of reports showing retinal implants capable of helping some participants perform simple tasks of daily living, such as detecting lights, recognizing objects and even reading large letters (6-9), the visual acuity of existing devices is very low, meaning that crucial abilities such as facial recognition are not yet possible.

One major cause for low visual acuity is the limited spatial resolution achievable through electrical stimulation with existing retinal implants. Ideally, to restore natural vision, each retinal neuron has to be stimulated individually and there are over 1.5 million retinal ganglion cells (RGCs) in the human retina (10). However, the electrode size of current retinal implants is usually much larger than the size of retinal neurons and the electrode number is low. For example, while the largest RGCs found in retina have a soma diameter of about 30 µm (11), Argus II only has 60 electrodes, each with a diameter of 200 µm (4), and the BVA suprachoroidal device only has 20 electrodes with diameters of 500 µm (6). Therefore, in striving for higher visual acuity, one logical approach is to develop devices made from arrays with many more, small, closely spaced electrodes.

In addition to increasing electrode density, carefully chosen stimulation patterns have been shown to improve visual acuity. For example, when using biphasic stimulation, varying pulse durations can refine the stimulation area for epi-retinal implants (12, 13). Previous research (12, 13) indicates that the spread of retinal ganglion cell activation via epi-retinal stimulation was dominated by the activation of passing axon bundles. Sub-retinal stimulation is expected to minimize such problems due to the larger separation between the sub-retinal stimulating electrodes and the axon bundles. However, no experimental evidence is yet available to show this difference. There is also evidence, both experimentally and in simulation, indicating that current focusing methods could improve spatial resolution (14-26).

Using nanostructured diamond electrodes, monolithically integrated with polycrystalline diamond housings, we previously reported the successful fabrication of an all-diamond hermetic electrode array with high electrode density (27, 28). This diamond array is composed of 256 electrodes, each 120 × 120 µm in size and with an electrode pitch of 150 µm (i.e. centre-to-centre distance). We have also previously demonstrated that the charge injection capacity of conductive diamond can reach more than 1 mC/cm$^2$ (29), much higher than in conventional metal materials such as platinum (150 µC/cm$^2$) (30). Owing to diamond's high chemical and biochemical inertness, as well as its excellent biocompatibility and electrochemical properties, the diamond implant device is expected to perform safely with high efficacy and long-term stability (29, 31-36).

In the present work, using a diamond electrode array, we first studied the effect of stimulation parameters (mainly pulse duration for biphasic stimulation) on the spatial resolution of sub-retinal implants using explanted retinas from wild type animals (Long Evans rats). Using a simple and effective method for loading calcium indicators into the RGCs of explanted adult rat retina, the responses of RGCs were recorded using fluorescence imaging techniques during electrical stimulation. To further confine the number of stimulated RGCs when multiple electrodes were stimulated simultaneously, we then implemented a novel return electrode, which surrounds each stimulating electrode on the array at a very close spacing. Our results suggest that biphasic stimulation with pulse durations as short as 0.1 ms, together with the use of the local return electrode are the most effective for confining the stimulation area for sub-retinal prostheses. The effects of stimulation were compared between normal and degenerated retinas, using Royal College of Surgeons (RCS) rats as the degenerated model.

## 2. Materials and Methods

### *2.1 Diamond Electrode Array Fabrication*

Since the focus of the present work is to reduce the activation area generated by single stimulation electrodes, instead of the full 256 electrode array described previously (27), we fabricated diamond arrays with 5 × 5 electrodes,

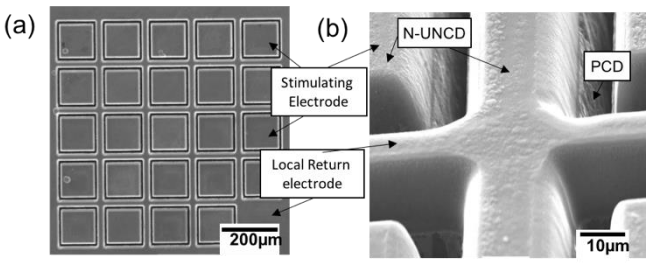


***Figure 1. SEM images of the diamond based microelectrode array for sub-retinal stimulation.*** *N-UNCD is the conductive diamond for stimulation and PCD is the insulating diamond. The local return electrode was fabricated by sacrificing the 25$^{th}$ electrode in a 5x5 electrode array and shorting it to all the non-stimulating areas, as shown in (a). (b) An enlarged area on the array, illustrating the separation between stimulating electrodes and the return area.*

where each electrode was a 120 × 120 µm square separated by a pitch of 150 µm. Briefly, 10 µm diameter feedthrough holes were cut through 5 × 5 × 0.5 mm polycrystalline diamond wafers (TM100 grade, Element Six Ltd) using an Oxford Lasers Alpha series laser micromachining system fitted with a Nd:YAG nanosecond pulse laser operating at 532 nm. Graphitic cutting residues were removed by 60 minutes exposure to boiling acid (10mL $H_2SO_4$ with 1g $NaNO_3$). 30 µm thick N-UNCD was grown within the feedthrough holes and over the array face by microwave chemical vapor deposition using a gas mixture of 20% $N_2$, 79% Ar and 1% $CH_4$, at a stage temperature of 850˚C, microwave power at 1000 W, and chamber pressure at 80 Torr. Following N-UNCD deposition, individual electrodes were isolated from one another by laser milling through the N-UNCD films and slightly into the PCD substrate, followed by a 24 hour oxygen plasma cleaning of graphitic residues. One out of 25 electrodes was sacrificed as a return electrode, shorted to all of the conductive diamond area surrounding the stimulating electrodes (Figure 1). Finally, silver active braze alloy (Morgan) was melted into the feedthrough pits in the PCD substrate and the diamond array was flip-chip bonded onto a custom designed circuit board to allow connection to a commercially available stimulator, as described previously (28, 37, 38) .

### *2.2 Retinal Preparation and Calcium Indicator Loading*

All procedures performed in this study were in accordance with the ethical standards of the Animal Care and Ethics Committee of The University of Melbourne. Data were acquired from adult pigmented Long Evans rats and Royal College of Surgeons (RCS-p+) rats, of either gender and older than 3 months. The RCS rat has inherited retinal degeneration and is widely used for research in hereditary retinal dystrophies. RCS rats completely lose their outer nuclear layer (39) as well as RGC light responses (40) after 90 days from birth. Animals were anesthetized with an intraperitoneal injection of a mixture of ketamine (7 mg/kg) and xylazine (10mg/kg), and then enucleated. After enucleation, 0.5 µl of 20 mM Oregon Green 488 BAPTA-1 solution (OGB-1, Hexapotassium salt, Thermo Fisher Scientific, dissolved in deionised water) was injected into each eye using a 10µl Hamilton syringe (Model 701N) from the cut end of the optic nerve (Figure 2a). The lens and cornea were then carefully removed and the retina was kept in an eyecup in a dish filled with carbogenated Ames' medium (Ames' medium 8.8 g/L, 23 mM $NaHCO_3$, 10 mM D-Glucose; all Sigma Aldrich) overnight at room temperature. Animals were sacrificed by intracardiac injection of 1ml of Lethabarb immediately after enucleation of the eyes. On the second day, the whole-mount retina was prepared by removing the eye-cup and cleaning the vitreous. In each set of experiments, half or one third of the retina was mounted with the photoreceptor side down in contact with the diamond microelectrode array and RGC side up (Figure 2b). The retina was held in place with a stainless steel harp fitted with Lycra threads (SHD-25GH, Warner Instruments, Hamden, CT). In all experiments, the stimulating electrodes were kept about 2.5 mm away from the optic nerve. The diamond array formed the bottom of a custom-made perfusion chamber, which was subsequently placed under an upright confocal microscope for visualization. The chamber was continuously perfused with carbogenated Ames' solution at a rate of 3-8 ml/min at physiological temperature (35-37 ˚C). At the end of the experiments, to reveal any damage to the RGCs, Sulforhodamine 101 (SU101, Sigma Aldrich) was added into the perfusion at a concentration of 10 nM.

In some of the experiments, to block both excitatory and inhibitory input to the RGCs, a mixture of bath applied synaptic antagonists was added, as reported in previous publications (41): (all in µM, Sigma Aldrich), 20 CNQX, 50 APB, 1 strychnine, 50 picrotoxin and 50 L-APB. The blocking solution was perfused for at least 20 minutes before stimulation.

### *2.3 Calcium Imaging and Electrical Stimulation*

The calcium activity of RGCs was monitored through a confocal microscope (Olympus, FluoView FV1200) using either a 10× or 20× objective lens. The source of excitation was a 473 nm laser. Images of an area of either 318 × 318 µm or 633 × 633 µm were captured at a frequency of 7.8 Hz.

Electrical stimulation was delivered using the Ripple Neuro System via a Nano2+Stim headstage. Each stimulation consisted of a burst of 10 anodic-first, charge balanced biphasic current waveforms (Figure S1), delivered at a frequency between 8 to 60 Hz, with varying pulse durations ranging from 0.033 ms up to 50 ms, and a constant interphase duration of 0.033 ms (see full list of parameters in Table S1). Current with 5 to 10 different amplitudes was delivered but in each recording, the current amplitude was kept the same and the burst of stimuli was delivered every 2 s and repeated 10 times (Figure S1). There was a 6 s delay at the beginning of each set of stimuli and a marker signal was also sent from the Ripple Neuro System to the confocal microscope to allow synchronizing images with stimulus presentations. As an electrical return, we used either a Ag|AgCl wire placed 2 cm away from the stimulating electrode in the chamber (distant return) or the local return electrode on the array (local return).

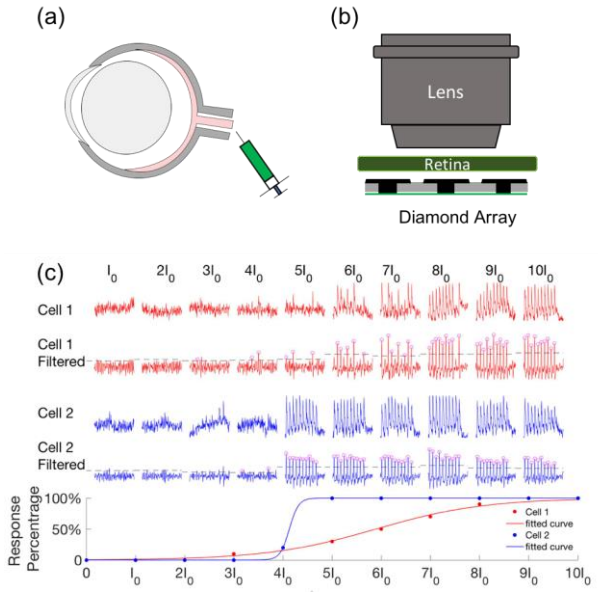


***Figure 2. Calcium imaging of RGCs in response to electrical stimulation.*** *In each experiment, calcium indicator OGB-1 was injected into the cut end of the optic nerve (a). After at least 6 hours of dye diffusion, retinas were mounted RGC side-up on a diamond electrode array and the responses to electrical stimulation were imaged. (c) Calcium transients of two example cells in response to different current amplitudes (from $I_0$ to $10I_0$) but with the same pulse duration. The stimuli were repeated 10 times with 2s intervals for each current amplitude. The response percentage was then measured after filtering the calcium transients and plotted as a function of current amplitude. The response was identified after thresholding at twice the standard deviation of the filtered data and then correlating temporally with the stimuli. A sigmoid function was fit to the data and a threshold current was defined at the amplitude giving a 50% response. The results shown in this figure were acquired from healthy, adult Long Evans rats.*

### *2.4 Data Analysis*

For each retina, stimulation of different pulse durations was repeated with at least 10 different current amplitudes and multiple areas on the retina were imaged to fully capture the whole stimulated region. The images were then stitched together using the MosaicJ (42) plugin in Fiji. Subsequently, the location of each ganglion cell body was determined manually according to the fluorescent standard deviation along the recording period, using the Fiji ROI tool. Electrically evoked responses were detected by first filtering the fluorescence intensity of each RGC, then thresholding at twice the standard deviation of the filtered data and finally identifying any rapid temporal changes in fluorescence that happened within 2 time windows (~0.26ms) following the onset of pulses. Filtering was performed by convolving the signals with a difference filter, [2 1 −1 −2](12). We plotted the response percentage of every RGC activated as a function of stimulus amplitude and fit a sigmoidal function (Figure 2c). The stimulation threshold was defined as the amplitude that activated 50% of the cells.

Spatial threshold maps were generated by binning cells in a grid according to their location relative to the stimulating electrode. Thresholds of cells in each grid bin (30 µm x 30 µm) were averaged. Maps from separate retinas or from different fields of view in the same retina were combined by rotating and shifting each into the same reference frame (relative to the optic disc and electrode position) and averaging. Each spatial threshold map was generated from at least three different retinas. Estimated diameters of activated areas for different pulse durations and return configurations were estimated according to the locations of RGCs activated with the average threshold currents in each experiment. The stimulated RGCs are first fitted with a 95% confidence ellipse by solving the covariance matrix made of the RGCs coordinates. The diameters reported are calculated from the circles that have the same areas as the fitted ellipses. For statistical analysis, student t-tests were performed to obtain the level of significance in Figure 6a and 8. All data processing was performed in Fiji (National Institutes of Health) (43) and MATLAB (MathWorks).

## 3. Results

### *3.1 Calcium Imaging of Retina*

To reveal the calcium ion activity of rat RGCs, 0.5 µl of calcium indicator Oregon Green 488 BAPTA-1 solution (OGB-1, 20 mM, dissolved in DI water) was injected from the severed end of the optic nerve following enucleation, as shown in Figure 2a. At least 6 hours of dye diffusion was found essential for high quality staining of the RGCs of whole retinas. Retinas were then loaded, RGC side-up onto a custom-made diamond electrode array arranged in a 5 × 5 square grid, where each electrode was a 120 × 120 µm square separated by a pitch of 150 µm. Explanted retinas were perfused with carbogenated Ames' medium and imaged with an upright confocal microscope with a 10× or 20× lens (Figure 2b). Figure 3a shows a segment of retina following overnight dye diffusion with the staining of RGCs, axon bundles and blood vessels. Except for the area close to the optic nerve where OGB-1 was injected, the staining was uniform across the retina.

The electrical stimulation was delivered sub-retinally through single diamond electrodes, mostly with a distant Ag/AgCl return electrode placed 2 cm away from the stimulating electrode. Depending on the testing stimulation parameters, experiments with the same piece of retina could last up to 4 hours. To reveal the health of retinas, at the end of the experiments, Sulforhodamine 101 (SU101) was added into the perfusion solution at a final concentration of about 10 nM to stain damaged RGCs, blood vessels and other extracellular space. Figure 3b-d shows retinal tissue following 4 hours of imaging and stimulation with little

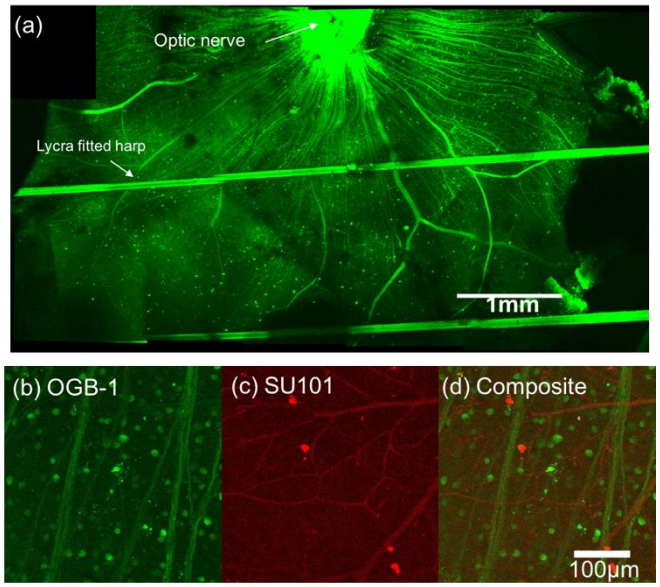


***Figure 3. Staining of RGCs.*** *(a) shows the staining of RGCs in a segment of retina after overnight calcium indicator diffusion. In (c), SU101 was used to reveal any damaged neurons at the end of the experiment. The small amount of overlapping between OGB-1 and SU101 staining (c-d) indicates the health of the retina after imaging and stimulation.*

overlap between OGB-1 and SU101 staining, indicating that most OGB-1 stained RGCs were alive and healthy at the end of the experiment. On average, less than 10% of the RGCs were found damaged at the end of the experiments.

Examples of two cells responding to biphasic stimulation with the same pulse duration but different currents are shown in Figure 2c. In this experiment, 10 different current amplitudes (from $I_0$ to $10I_0$) were delivered with 10 repeats at an interval of 2 s. In all experiments, the maximum current amplitudes were determined according to the maximum diamond charge injection capacity (1500 μC/cm$^2$) or the maximum available current from the stimulator (1500 μA). Neurons showed an increase of fluorescence intensity when stimulated and the percentage of the maximum response was counted after convolving the recorded intensity with an additional filter. Finally, the relationship between the response percentages and current amplitudes were plotted and fitted with a sigmoid function. Threshold current was defined as the current at 50% of the maximum value of the fitted sigmoid.

### *3.2 The Effect of Different Pulse Durations*

Long Evans rats with healthy retinas were used to assess the relationship between pulse duration and response. The neurons were identified manually with Fiji (43) and placed into 30 × 30 μm square grids based on their locations (Figure 4). The colour code used for each grid indicates the average thresholds for all activated cells in that grid (see Materials and Methods). In this way, we present a summary of the spatial response of retinas to different pulse durations, ranging from 0.033 ms up to 50 ms (Figure 4) using the distant return configuration. The detailed stimulus parameters are plotted in Figure S1 and listed in Table S1. The size of each circle depends on the number of neurons in each grid and the 120 × 120 μm stimulation electrode is drawn as a blue square in the images. Each threshold map was an average of at least three pieces of retina stimulated with the same parameters. The maps are oriented so that the optic nerve is to the left side of all images.

The results show that stimulation led to activated cells across larger areas when using medium length pulse durations (0.2 ms to 8 ms). In addition to the areas on top of and around the electrodes, neurons as far as 800 μm away from the electrode centers were activated. When using pulse durations longer than 8 ms, the spread of the stimulation was also significant. However, neurons far away from the electrodes were stimulated with smaller charges than neurons on top of the electrodes, regardless of the relative location of the return electrode. The stimulation was mostly confined within the boundaries of the electrodes when pulse durations were below 0.2 ms. With a pulse duration of 0.033 ms, only neurons on top of or close to the electrodes were stimulated. The diameters of the stimulated areas in each experiment using the average threshold charge are plotted in Figure 5, which quantify the trends shown by the threshold maps.

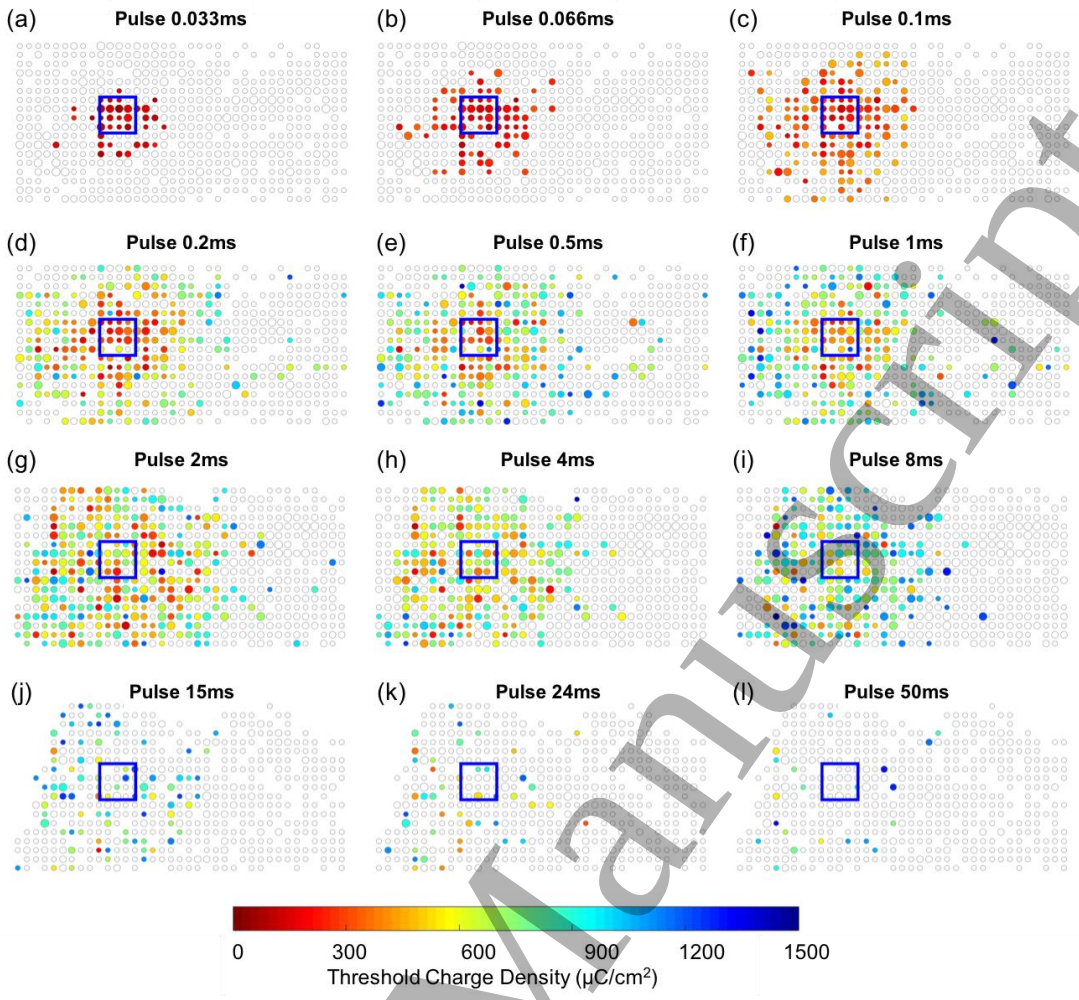


***Figure 4. The effect of different pulse durations on the spatial resolution of sub-retinal stimulation.*** *All results shown in this figure were collected using a distant return electrode using healthy retinas. The detailed stimulus parameters are listed in Table S1. The 120μm x 120μm electrode is shown as the blue square in the images. Each colored dot represents the average threshold charge density needed to stimulate cells at its location. Unfilled grey dots indicate areas containing cells that did not respond to stimulation. Small, medium and large dots specify one to two, three to four and five or more cells, respectively. Maps are oriented such that the optic disc lies to the left of the image, with axons running horizontally toward their originating somas on the right. Each map contains data from at least three retinas.*

We hypothesized that larger spread is associated with network activation, so we blocked synaptic transmission from other neurons to RGCs. Figure 6a shows the change of stimulation thresholds before and after the application of blockers. For direct comparison, the synaptic experiments were conducted using the same piece of retina with the same stimulating electrode and in the same imaging areas. In order to complete the data collection for all pulse durations, both before and after adding synaptic blockers within one single experiment, imaging was performed within a small area and we focused on the change in stimulating thresholds instead of the spread of activation. When stimulating without synaptic blockers, the threshold charge density increased with pulse duration. After adding the synaptic blockers, the average threshold charge density increased in all cases and the

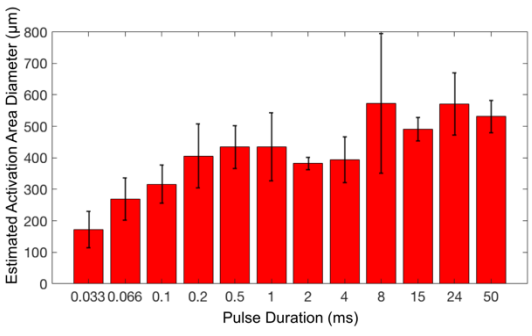


***Figure 5. Estimated activated area with different pulse durations using a distant return electrode and healthy retinas.*** *The areas were estimated when stimulating with the average threshold.*

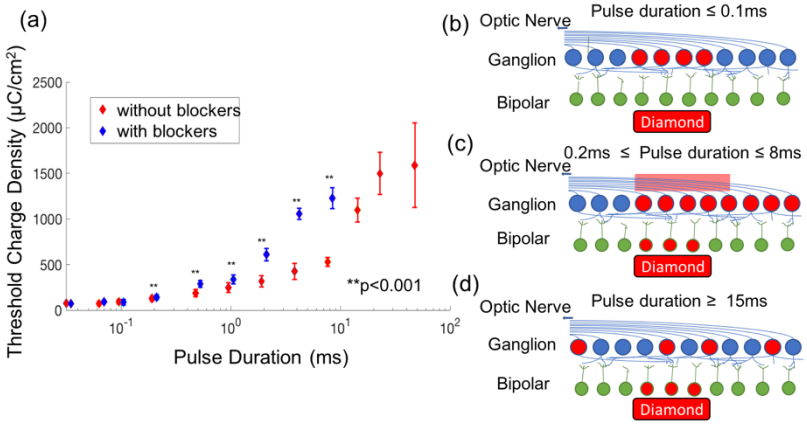


***Figure 6. Possible effects of pulse duration on spatial resolution.*** *(a) The different average charge thresholds of RGCs that were activated with or without the presence of synaptic blockers. With synaptic blockers, no RGCs could be activated with pulse durations larger than 8ms. For pulse durations larger than 0.2ms, thresholds rose significantly when blockers were applied (paired student t-test **p<0.001). A schematic of the possible effects of pulse durations on spatial resolution is summarized in (b-d). Neurons and axon bundles that are activated by electrical stimulation are drawn as red. For pulse durations smaller than 0.1ms, sub-retinal electrodes directly activated the RGCs. When pulse durations of 0.2ms-8ms were applied, the RGCs were activated both directly and indirectly through axon bundles and the retinal network. The pulse durations larger than 15ms mainly stimulated RGCs through the retinal network.*

threshold went so high that no neurons could be activated within the safe range for diamond-charge injection when using pulse durations longer than 8 ms. Based on a statistical analysis(Figure 6a), the threshold increase was significant for pulse durations between 0.2 ms and 8 ms. Although the average thresholds also increased for shorter pulse durations, there was no statistical difference between the thresholds.

The experiments with synaptic blockers most likely indicate that different types of neurons were activated when different pulse durations were used (Figure 6). Since synaptic blockers did not change the thresholds significantly for short pulse durations (≤0.1 ms), most of the RGCs were probably activated directly. The difference observed between 0.033 ms and 0.1 ms was possibly due to the different maximum charge available from the stimulator used in this study. As the maximum available current was 1500 μA, the maximum injectable charge was 343 μC/cm2 for 0.033 ms and 1031 μC/cm2 for 0.1 ms. The activation area increased for 0.1 ms as more charge could be injected. For very long pulse durations (≥15 ms), the RGCs were most likely activated through other neurons in the retinal network, such as bipolar cells and amacrine cells. Many rat RGCs have large dendrites and some of the dendrites can be as large as 500 μm in diameter (44). Therefore, even if the electrodes activate neurons other than RGCs very close to their centers, the soma of the indirectly activated RGCs may be hundreds of micrometers away. With long pulses, we also observed a larger variability of thresholds among neurons, as indicated by the error bar representing the standard deviation. For medium length pulse durations, RGCs could be stimulated both directly from the electrodes and indirectly from the other neurons. Furthermore, the activation of neurons further away from the optic nerve, forming the streak shape, also indicates the activation of axon bundles, which lead to the further spread of cell activation.

### *3.3 The Effect of Return Electrode Type and Location*

The results above indicate that shorter pulse durations are beneficial for spatial confinement of the region of the stimulation of sub-retinal devices. However, when using very short pulse durations such as 0.033 ms, the threshold current is normally larger than 500 μA and possibly higher than what is available from the implanted application specific integrated circuits (ASIC) (45, 46). The large current will also consume more instantaneous power, leading to energy storage challenges. Previous reports, both experimentally and in simulation, indicate that the use of local return electrode configurations can also be beneficial for improving the spatial resolution of the stimulation (14-26). With the hope of reducing the threshold current as well as improving the spatial resolution, here we tested the effect of different return locations but with pulse durations of 0.1 ms, 0.5 ms and 2 ms.

Both the distant and a local return electrodes were applied and compared. The local return was created by shorting all the non-stimulating electrode areas on the face of the array (Figure 1). Figure 1b shows an enlarged image of the area between stimulating electrodes where a 10 μm wide groove was created using laser scribing, removing the conductive diamond and isolating the electrodes from one another electrically, while 10 μm ridges between electrodes were applied as electrical returns. The distant return electrode was placed approximately 2 cm away from the stimulating electrodes in the perfusion chamber, as described above.

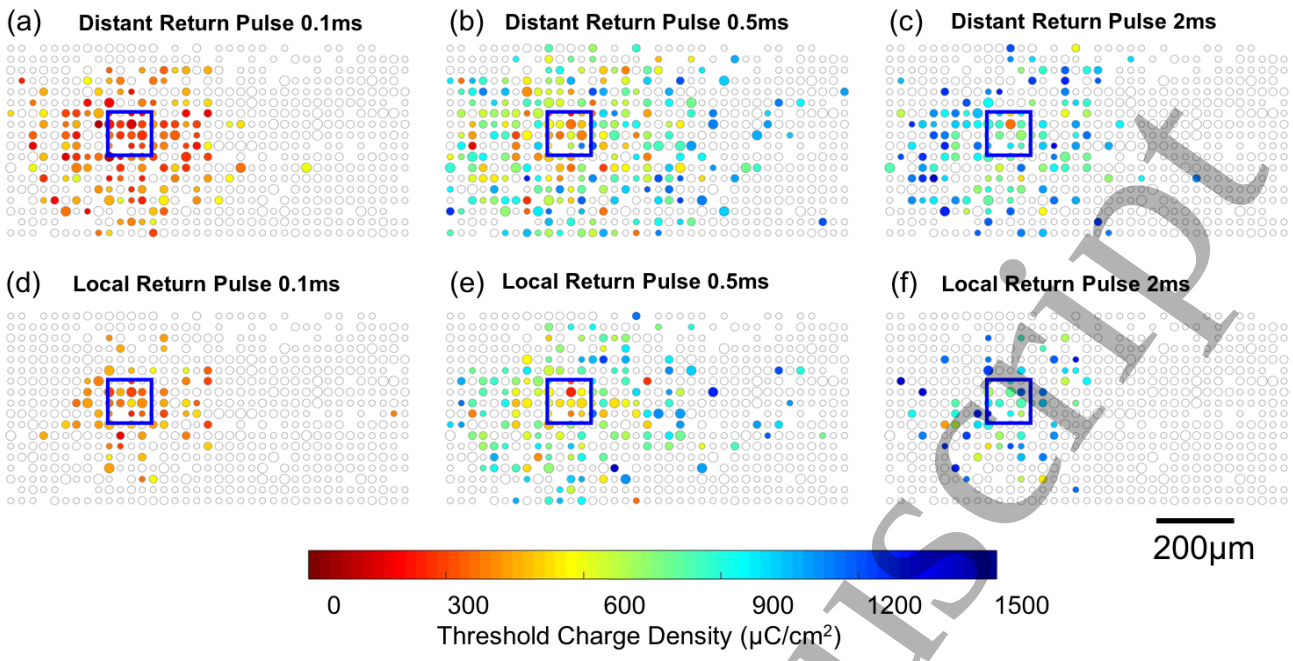


***Figure 7. Effects of different return configurations with healthy retinas.*** *The spatial threshold maps reveal that the stimulation areas were smaller for pulse durations of 0.1ms and 2ms.*

Figure 7 shows the summary of the results with pulse durations of 0.1 ms, 0.5 ms and 2 ms. The threshold maps were composed of retinas in which both local return and distant return configurations were tested. When using local return electrodes, the thresholds for 0.1 ms pulses increased by 11.7% while the thresholds for the other two pulse durations showed no significant change (Figure 8a). The variance between retinas was found to be similar for different electrode configurations and in the case of retinal degeneration. In general, the average areas that exhibited activated cells were much smaller for both 0.1 ms and 2 ms duration pulses, with significant differences observed for 2ms duration pulses (Figure 8b). However, the effect of activated area between the distant and local return electrodes for pulse durations of 0.5 ms were not obvious.

### *3.4 The Effect of Retinal Degeneration*

The above experiments were conducted with wild type animals. Since retinal implants are intended for the treatment of retinal degeneration, we repeated the experiments with retinas from RCS rats (Figure 8,9). RCS rats older than 3 months have been previously demonstrated to have complete loss of photoreceptors and sight, therefore, they are a standard animal model for studying retinal degeneration (47). We found a decrease of RGC density in RCS rats that is about 80% of the density in wild type retinas. The thickness of retina is also expected to be different between RCS and wild type rats ( > 200 μm in Long Evans and <150 μm in RCS (48) ). When comparing the threshold differences between normal and degenerated retinas (Figure 8a), the charge threshold densities were found to be smaller in degenerated retinas for pulse durations shorter than 2 ms, with either distant or local returns. These results are not consistent with previous reports which found similar or elevated stimulation thresholds in degenerated retinas (12, 39, 40, 49-51) (see Discussion). However, when a pulse duration of 24 ms was applied, the threshold was significantly higher for degenerated retinas. Among three RCS retinas tested in this work, only one RCS retina responded to stimuli with a 24 ms pulse duration. In terms of the spatial resolution (Figure 9), similar to results from wild type animals, both medium and long pulse durations led to a larger spread of activated cells, while the activated area was most confined for the electrodes when using the shortest pulse durations (0.033 ms).

The experiments were also repeated with different return electrode locations. From the threshold maps, the local return did not result in differences in activation areas from any of the pulse durations applied (0.1 ms, 0.5 ms and 2 ms) (Figure 9). However, the diameters of the activated area when using the average thresholds (Figure 8b) were smaller for all RCS retinas stimulated with 0.1 ms when a local return was applied, indicating that the local return could potentially reduce the activating area in RCS retinas, although not as effectively as that in healthy retinas.

## 4. Discussion

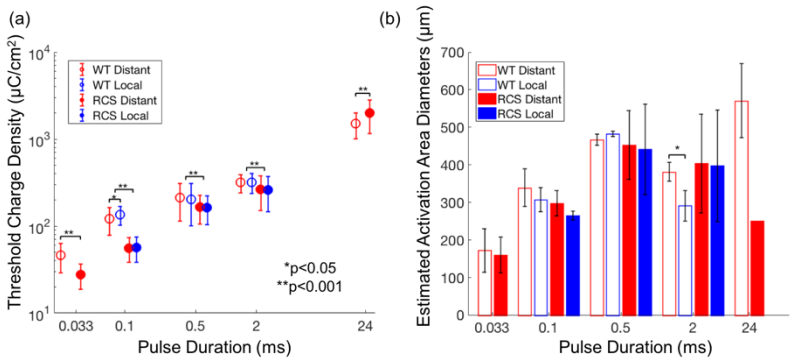


***Figure 8. the effect of different return configurations and retina degeneration on the threshold charge density (a) and estimated activation area diameters (b).*** *(WT: wild type rats; RCS: Royal College of Surgeons rats)*

Calcium imaging has been used previously to study the possible spatial resolutions that can be achieved with retinal implants *in vitro* (52-56). Behrend et al. (52) first reported large area loading of RGCs with calcium indicators by immersing the optic nerve stumps in dye solution but this protocol was found to be unsuccessful with adult mammal retinas (52, 56). Multicell bolus loading with membrane-permeable indicators was also reported but uniform staining was not achieved (53). Briggman and Euler (54) successfully stained large numbers of RGCs in adult mammalian retina with bulk electroporation. Although this approach could result in over 92% of RGC staining with less than 1% of the cells damaged, an extremely careful control of electroporation parameters is necessary (which we found difficult to repeat consistently). Another method that has been reported for staining large numbers of RGCs is to transduce the cells with genetically encoded calcium indicators through adeno-associated viral vectors (56). With this method, a 2-4 week waiting period is necessary before high quality expression. The approach used here for uniform staining of RGCs by injecting the cell membrane impermeable calcium indicators directly into the optic nerve after enucleation proved relatively easy to perform without risk of damaging the targeted cells. Furthermore, the loading time (at least 6 hours) is significantly shorter than when using genetically encoded calcium indicators.

There are several limitations in our study due to the imaging technique we used for recording the responses of RGCs to electrical stimulation. Firstly, calcium transients from single action potentials were difficult to detect and trains of stimulus pulses had to be applied, as previously reported (12, 17, 56). Therefore, it is possible that the RGCs were being activated but the number of activated action potentials was too small to detect calcium transients. To obtain detectable fluorescent transients, a group of pulses was used at a frequency of 60Hz for most of the pulse durations (see full stimulation parameters in Table S1). Previous research indicated that it is difficult for network-mediated responses to follow repetitive stimulation at such high frequencies (57). Therefore, the stimulation frequency employed in this study would have limitations if attempting to study network-mediated responses. The excitation wavelength (473 nm) applied in this work for imaging also limits the ability to study the light responses of the retina (58). Selectively activating different types of RGCs has been an interesting topic in recent years (59-61). However, to determine the RGC types, two-photon microscopy is required, which we did not use (58). The low temporal resolution of the imaging technique employed here also limited our ability to distinguish between direct and indirect RGC activation based on response latency. With electrical recording, the direct RGC response is usually associated with spikes that occur within 5ms of the onset of electrical stimulation. Spikes recorded at longer latencies are associated with indirect network activation. The low scan rate (7.8 Hz) of our imaging system was too slow to distinguish between direct and indirect activation. Another limitation of this study lies in the non-transparency of diamond electrodes, which made it impossible to image the cells during epi-retinal stimulation because the fluorescence was blocked when the electrodes were between the retina and the objective lens. To image the responses to epi-retinal stimulation, we also attempted to image the RGCs through the retinal tissue with the photoreceptor side upwards in the microscope. However, this has proved problematic due to the thickness of the tissue between the object lens and the RGCs.

Varying the durations of electrical stimulation pulses is essential for determining both the temporal and spatial responses of RGCs to electrical stimulation (12, 13, 62-66). Consistent with previous studies (12, 13, 62-66), we showed that RGCs responded differently when exposed to different pulse durations. Generally, we found that with sub-retinal stimulation very short stimuli (pulse durations <=0.1 ms) tended to directly stimulate RGCs while longer stimuli (pulse durations >=15 ms) tended to indirectly stimulate RGCs through the retinal network. With medium length stimulation, RGCs can be stimulated directly and indirectly through both the retinal network and axon bundles. Indirect stimulation could lead to large activation patterns due to either the large dendrites of RGCs or due to stimulation of passing axon bundles. Therefore, shorter stimulation led to the most confined activation patterns of RGCs.

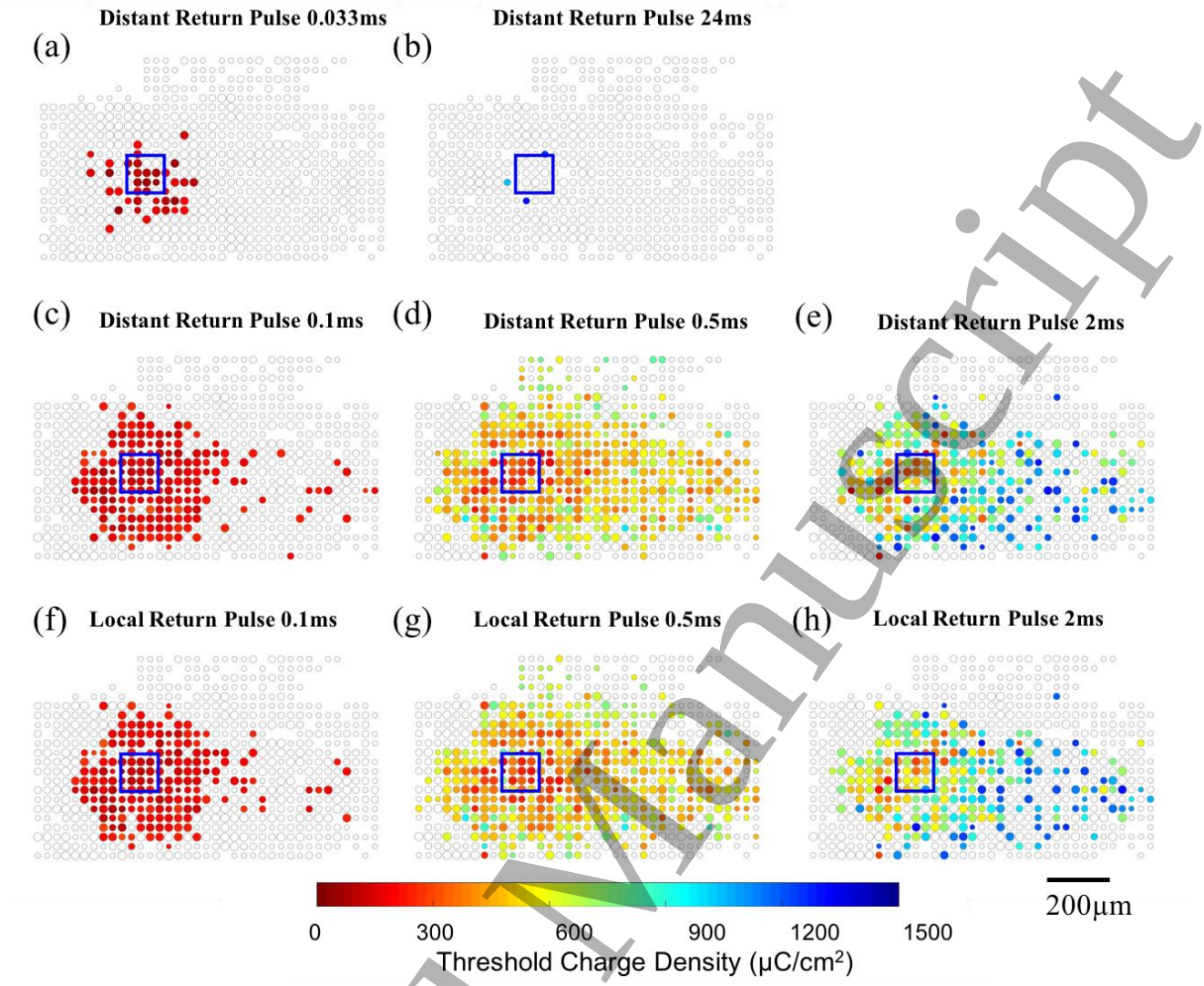


***Figure 9. The effect of retinal degeneration on the spatial resolution of sub-retinal stimulation.*** *The threshold maps of degenerated retinas for distant returns with pulse durations from 0.033ms to 24ms are summarized in a-c. The experiments were also repeated with local returns for pulse durations of 0.1ms, 0.5ms and 2ms (f-h).*

Similar studies using different pulse durations have been reported, but all with epi-retinal stimulation (12, 13). For example, Weitz et al. suggested the use of longer pulse durations to avoid activation of axon bundles because longer pulses tend to indirectly stimulate RGCs through the retinal network (12). Compared with epi-retinal stimulation, in our work with sub-retinal stimulation, we found the activation of axon bundles to be less of a problem for the spread of activation when we used pulse durations of less than 0.1 ms. Importantly, the activation of axon bundles with these short durations was insignificant compared with the results with medium length pulses. This finding, although different from Weitz et al (12) , is consistent with many other reports that used epi-retinal stimulation. For example, Jensen and Rizzo III (65) recommended pulses of 0.1 ms or less to avoid the activation of passing retinal ganglion cell axons. By choosing these short pulse durations, the amount of current needed to generate a response from a cell was much lower than that required to generate an axonal response. Chang et al. also suggested the use of pulses shorter than 0.12 ms to avoid axon bundle stimulation (13). In another study from Grosberg and colleagues, 45% of the electrodes in the peripheral retina activated individual RGCs without activating bundles (67). In that study, they used triphasic current pulses with a total duration of 0.15 ms. In our study, the fact that the stimulating thresholds for RGCs did not increase significantly for short pulses after application of synaptic blockers (Figure 6a) indicates that the RGCs were mainly stimulated directly. The increase of activation spread observed from 0.033 ms to 0.1 ms is likely due to the

different maximum charge injected from the stimulator. As the maximum current available from the stimulator is 1500 µA, the maximum amount of charge injected was different when using 0.033 ms and 0.1 ms pulses. When using long pulses, we found the activation of RGCs was mainly through the retinal network and the spread of activated cells was still large, possibly due to the large dendrites of RGCs. Compared with epi-retinal implants, sub-retinal stimulation normally aims to activate cells in the inner layers and not the RGCs, with the hope that by stimulating the retinal network prior to the RGCs more natural processing mechanisms might be engaged. However, retinal remodeling has been reported in degenerated retinas and the responses of RGCs to network stimulation have been found to be different between wild type animals and those with retinal degeneration. There are additional practical problems associated with network stimulation. For example, the temporal resolution of network stimulation is low and image fading during stimulation has long been believed to be associated with network stimulation (66, 68). Also the threshold charges for stimulation with long pulses can be larger than 1 mC/cm$^2$, as shown in Figure 4. The large charge required will consume greater amounts of power and may also exceed the safe charge injection limit of conventional electrode materials, such as platinum (150 µC/cm$^2$) (30). Therefore, there are some advantages in trying to optimize direct RGC activation even with sub-retinal implants.

Although ultrafast pulses can produce localized stimulation of RGCs, the current amplitudes required to induce activation during short pulses is normally quite high. For example, the thresholds when using 0.033 ms pulses can be larger than 500 µA. These large currents are beyond the capability of most of the implanted electronic circuits used to drive stimulation (45, 46). Moreover, such currents are inefficient in terms of the instantaneous power required. Therefore, in addition to studying the effects of different pulse durations, we also looked at the effects of different return locations. For cochlear implants, local returns have been used to reduce electrical crosstalk (69), although sometimes at the expense of higher thresholds and lower dynamic range. The use of local return configurations has been suggested by many groups as a method for improving the spatial resolution of retinal implants (14-18, 20, 21, 24-26). In our work, the local return electrode surrounded the stimulating electrodes and the gap between the return and stimulating electrodes was only 10 µm in width. Analogous configurations include switching other stimulating electrodes in the arrays into return electrodes. In both simulations (14, 17, 18, 23, 25) and experiments (15, 16, 19-22, 24, 26), there were two major observations when using local return configurations: the electrical activation area can be confined and the threshold for stimulation is higher when compared with the results from stimulating with a distant return electrode. However, for most of the simulations, the models were simplified by assuming isotropy of the tissue and only considering electrostatic effects (14, 18, 23, 25). Some of the models did not include any tissue activation (18, 25) and for the others, they only took into account RGC activation and did not consider the effects of axon bundle or network stimulation (14, 23). In experiments, the *in vitro* recordings were conducted either with single unit extracellular recordings (15, 19) or patch clamp recordings (20), while the *in vivo* recordings (16, 26) were mostly performed with low density multielectrode arrays in visual cortex. None of the previous recording techniques were able to provide spatial resolution as high as the imaging method employed in our study and rarely did they take the effect of pulse duration into consideration.

In our experiments, we found that the effects of the return configurations depended on the pulse duration, which is likely due to the susceptibility of retinal components to different pulse durations. When the retina was stimulated with fast pulses (0.1 ms), the activation of RGCs was mostly from direct electrical stimulation of the somas. Therefore, as expected from simulations, the activated areas decreased and the average thresholds increased 11.7% when switching from the distant return to the local return. However, the current necessary for stimulating RGCs with 0.1 ms in the local return configuration is still smaller than the current required with 0.033 ms with the distant return. When medium length pulses (0.5 ms and 2 ms) were employed, the effects were much more complicated as both direct and indirect activation of RGCs occurred simultaneously. We did not observe significant changes of thresholds but when stimulating with 2 ms pulses, we did observe a reduction in the area activated with the local return. However, to translate the local return configuration into clinical trials, further *in vivo* testing needs to be performed to confirm the effects. For example, while Cicione et al. found that local return configurations yielded narrower spreads of retinal activation, this did not translate to more focused cortical activation (16).

The effect of retinal degeneration was studied by applying the same stimuli to retinas from RCS rats older than 3 months. These retinas have completely lost their photoreceptors (47), which is representative of the late stages of retinitis pigmentosa. We found that the average thresholds for RGCs activation in degenerated retinas differed from the wild type (Figure 4c). For pulses shorter than 2 ms, there was less charge required for activating RGCs in RCS retina. As shorter pulses tend to directly stimulate RGCs, retinal degeneration may lead to smaller distances between RGCs and sub-retinal stimulating electrodes (> 200 µm in Long Evans and <150 µm in RCS (48)), which could decrease thresholds for RGC stimulation. However, when network stimulation becomes the dominant component for RGC

activation, as is the case with 24 ms pulses, the RGC threshold increased significantly with retinal degeneration. This is likely due to the loss of photoreceptors and other retinal neurons, as well as the retinal remodeling that occurs during degeneration (70). Previous studies found that the thresholds for activation of RGCs increase or stay the same following retinal degeneration (3, 39, 40, 49, 51, 67). However, in the studies showing elevated thresholds (39, 49, 51), pulse widths applied could excite both ganglion cells and other neurons in the retina. This is consistent with the increased thresholds observed in our study when using long pulses. For the other studies reporting unchanged thresholds following degeneration, the stimulus parameters were chosen to ensure direct RGC stimulation but delivered epi-retinally (12, 40, 50), where the distance between electrode and RGCs were kept the same for both degenerated and healthy retinas. This may account for the different observation in our study because in the case of sub-retinal stimulation, the distance between the electrodes and the RGCs decreases when degenerated retinas are used.

The effect of pulse duration on the spatial resolution of sub-retinal stimulation of degenerate retina was found to be similar to that of normal retinas. The shortest pulse (0.033 ms) resulted in the most confined stimulation patterns. In degenerate retinas, when pulses between 0.1 ms and 2 ms were utilized, more RGCs were activated through axon bundles than those in normal retinas, indicating a lower threshold for axon bundle stimulation in degenerate retinas, possibly due to the smaller distance between axon bundles and electrodes. When using 24 ms pulses, the RGC thresholds were so high that few neurons could be activated.

We only observed small differences when changing the return electrode location with degenerate retinas, as compared to normal retinas (Figure 8, 9f-h). Simulation results indicate that the impact of return electrode locations is more significant when the distance between the electrodes and RGCs increases (25), which may account for the observations made in degenerate retinas. Retinal thickness in human RP patients varies depending on the stage of the disease (71). Retinal thickness of less than 100 µm has been reported in some patients, which is even smaller than the retinal thickness of RCS rats (~ 150 µm) (48). Therefore, in clinical trials, for sub-retinal implants, changing the return configurations may not have much advantage. However, it indicates that the local return may have more potential to improve spatial resolution when the electrodes are implanted further away from the retina, e.g. in a suprachoroidal location (between the sclera and choroid of the eye) or in the epi-retinal space. Compared with sub-retinal and epi-retinal devices, suprachoroidal implants provide significant surgical and safety benefits for patients, but suffer from low stimulating resolution due to the large distance between the electrodes and retina (6). For epi-retinal implants, there is also surgical difficulty in placing the electrode array close to the retina without inducing retinal damage. The design of local returns could possibly benefit both implant configurations by reducing the areas of activation from single electrodes.

## 5. Conclusion

In summary, we conducted calcium imaging on explanted retinas from both wild type rats and rats with retinal degeneration during sub-retinal electrical stimulation, and studied the effect of different pulse durations from biphasic stimulation and the impact of two return configurations. We found that the most confined pattern for RGC activation was achieved by direct RGC stimulation, although sub-retinal devices normally target the inner retinal neurons. With a distant return electrode, pulses shorter than 0.1ms were found to be effective for spatial confinement of the stimulation pattern for both healthy and degenerated retinas. To further reduce the spread of stimulation and minimize the threshold currents, a local return was employed and found to be effective only when using normal retinas with either 0.1 ms or 2 ms pulses. Further experiments will be conducted with multiple, simultaneous electrode stimulation.

## Acknowledgements

We thank the Melbourne Advanced Microscopy Facility housed within Bio21 at The University of Melbourne for SEM Imaging. The research was supported by a Development Grant from The National Health and Medical Research Council (NHMRC, GNT1118223) of Australia. The work was performed in part at the Melbourne Centre for Nanofabrication (MCN) in the Victorian Node of the Australian National Fabrication Facility (ANFF). DJG is supported by NHMRC Project Grant GNT1101717 and by an Australian Nanofabrication Facility (ANFF)/ Melbourne Centre for Nanofabrication (MCN) Technology Ambassador Fellowship. S.P. is cofounder and shareholder of iBIONICS, a company developing a diamond based retinal prothesis. S.P, D.J.G and N.V.A are shareholders and executive officers of Carbon Cybernetics Pty Ltd, a company developing diamond and carbon-based medical device components. The other authors declare no conflict of interest.

## References

1. Bourne RR, Stevens GA, White RA, Smith JL, Flaxman SR, Price H, et al. Causes of vision loss worldwide, 1990–2010: a systematic analysis. The lancet global health. 2013;1(6):e339-e49.

2. Taylor HR, Keeffe JE, Vu HT, Wang JJ, Rochtchina E, Mitchell P, et al. Vision loss in Australia. Medical Journal of Australia. 2005;182(11):565-8.
3. Goetz GA, Palanker DV. Electronic approaches to restoration of sight. Rep Prog Phys. 2016;79(9).
4. Dorn JD, Ahuja AK, Caspi A, da Cruz L, Dagnelie G, Sahel JA, et al. The Detection of Motion by Blind Subjects With the Epiretinal 60-Electrode (Argus II) Retinal Prosthesis. Jama Ophthalmol. 2013;131(2):183-9.
5. Stingl K, Bartz-Schmidt KU, Besch D, Chee CK, Cottriall CL, Gekeler F, et al. Subretinal Visual Implant Alpha IMS - Clinical trial interim report. Vision Research. 2015;111:149-60.
6. Ayton LN, Blamey PJ, Guymer RH, Luu CD, Nayagam DAX, Sinclair NC, et al. First-in-Human Trial of a Novel Suprachoroidal Retinal Prosthesis. Plos One. 2014;9(12).
7. Zrenner E, Bartz-Schmidt KU, Benav H, Besch D, Bruckmann A, Gabel VP, et al. Subretinal electronic chips allow blind patients to read letters and combine them to words. P Roy Soc B-Biol Sci. 2011;278(1711):1489-97.
8. Humayun MS, Dorn JD, da Cruz L, Dagnelie G, Sahel JA, Stanga PE, et al. Interim Results from the International Trial of Second Sight's Visual Prosthesis. Ophthalmology. 2012;119(4):779-88.
9. Stingl K, Bartz-Schmidt KU, Besch D, Braun A, Bruckmann A, Gekeler F, et al. Artificial vision with wirelessly powered subretinal electronic implant alpha-IMS. P Roy Soc B-Biol Sci. 2013;280(1757).
10. Harman A, Abrahams B, Moore S, Hoskins R. Neuronal density in the human retinal ganglion cell layer from 16-77 years. Anat Rec. 2000;260(2):124-31.
11. Liu ZL, Kurokawa K, Zhang FR, Lee JJ, Miller DT. Imaging and quantifying ganglion cells and other transparent neurons in the living human retina. P Natl Acad Sci USA. 2017;114(48):12803-8.
12. Weitz AC, Nanduri D, Behrend MR, Gonzalez-Calle A, Greenberg RJ, Humayun MS, et al. Improving the spatial resolution of epiretinal implants by increasing stimulus pulse duration. Sci Transl Med. 2015;7(318).
13. Chang YC, Ghaffari DH, Chow RH, Weiland JD. Stimulation strategies for selective activation of retinal ganglion cell soma and threshold reduction. J Neural Eng. 2019;16(2).
14. Abramian M, Lovell NH, Habib A, Morley JW, Suaning GJ, Dokos S. Quasi-monopolar electrical stimulation of the retina: a computational modelling study. J Neural Eng. 2014;11(2):025002.
15. Abramian M, Lovell NH, Morley JW, Suaning GJ, Dokos S. Activation of retinal ganglion cells following epiretinal electrical stimulation with hexagonally arranged bipolar electrodes. J Neural Eng. 2011;8(3).
16. Cicione R, Shivdasani MN, Fallon JB, Luu CD, Allen PJ, Rathbone GD, et al. Visual cortex responses to suprachoroidal electrical stimulation of the retina: effects of electrode return configuration. J Neural Eng. 2012;9(3).
17. Flores T, Goetz G, Lei X, Palanker D. Optimization of return electrodes in neurostimulating arrays. J Neural Eng. 2016;13(3):036010.
18. Gerhardt M, Alderman J, Stett A. Electric field stimulation of bipolar cells in a degenerated retina—a theoretical study. IEEE transactions on neural systems and rehabilitation engineering. 2010;18(1):1-10.
19. Gerhardt M, Groeger G, MacCarthy N. Monopolar vs. bipolar subretinal stimulation-An in vitro study. J Neurosci Meth. 2011;199(1):26-34.
20. Habib AG, Cameron MA, Suaning GJ, Lovell NH, Morley JW. Spatially restricted electrical activation of retinal ganglion cells in the rabbit retina by hexapolar electrode return configuration. J Neural Eng. 2013;10(3).
21. Matteucci PB, Barriga-Rivera A, Eiber CD, Lovell NH, Morley JW, Suaning GJ. The Effect of Electric Cross-Talk in Retinal Neurostimulation. Invest Ophth Vis Sci. 2016;57(3):1031-7.
22. Matteucci PB, Chen SC, Tsai D, Dodds CWD, Dokos S, Morley JW, et al. Current Steering in Retinal Stimulation via a Quasimonopolar Stimulation Paradigm. Invest Ophth Vis Sci. 2013;54(6):4307-20.
23. Moghaddam GK, Lovell NH, Wilke RG, Suaning GJ, Dokos S. Performance optimization of current focusing and virtual electrode strategies in retinal implants. Computer methods and programs in biomedicine. 2014;117(2):334-42.
24. Spencer TC, Fallon JB, Thien PC, Shivdasani MN. Spatial restriction of neural activation using focused multipolar stimulation with a retinal prosthesis. Invest Ophth Vis Sci. 2016;57(7):3181-91.
25. Wilke R, Moghadam GK, Lovell N, Suaning G, Dokos S. Electric crosstalk impairs spatial resolution of multi-electrode arrays in retinal implants. J Neural Eng. 2011;8(4):046016.
26. Wong YT, Chen SC, Seo JM, Morley JW, Lovell NH, Suaning GJ. Focal activation of the feline retina via a suprachoroidal electrode array. Vision Research. 2009;49(8):825-33.
27. Ganesan K, Garrett DJ, Ahnood A, Shivdasani MN, Tong W, Turnley AM, et al. An all-diamond, hermetic electrical feedthrough array for a retinal prosthesis. Biomaterials. 2014;35(3):908-15.
28. Ahnood A, Meffin H, Garrett DJ, Fox K, Ganesan K, Stacey A, et al. Diamond devices for high acuity prosthetic vision. Advanced Biosystems. 2017;1(1-2).
29. Tong W, Fox K, Zamani A, Turnley AM, Ganesan K, Ahnood A, et al. Optimizing growth and post treatment of diamond for high capacitance neural interfaces. Biomaterials. 2016;104:32-42.
30. Cogan SF. Neural stimulation and recording electrodes. Annu Rev Biomed Eng. 2008;10:275-309.
31. Garrett DJ, Ganesan K, Stacey A, Fox K, Meffin H, Prawer S. Ultra-nanocrystalline diamond electrodes: optimization towards neural stimulation applications. J Neural Eng. 2011;9(1):016002.
32. Garrett DJ, Saunders AL, McGowan C, Specks J, Ganesan K, Meffin H, et al. In vivo biocompatibility of

boron doped and nitrogen included conductive-diamond for use in medical implants. Journal of Biomedical Materials Research Part B: Applied Biomaterials. 2016;104(1):19-26.
33. Garrett DJ, Tong W, Simpson DA, Meffin H. Diamond for neural interfacing: A review. Carbon. 2016;102:437-54.
34. Hadjinicolaou AE, Leung RT, Garrett DJ, Ganesan K, Fox K, Nayagam DA, et al. Electrical stimulation of retinal ganglion cells with diamond and the development of an all diamond retinal prosthesis. Biomaterials. 2012;33(24):5812-20.
35. Tong W, Tran PA, Turnley AM, Aramesh M, Prawer S, Brandt M, et al. The influence of sterilization on nitrogen-included ultrananocrystalline diamond for biomedical applications. Materials Science and Engineering: C. 2016;61:324-32.
36. Shivdasani M, Garrett D, Nayagam D, Villalobos J, Allen P, Saunders A, et al. In vivo electrical stimulation of a retinal prosthesis containing conductive diamond electrodes. Investigative Ophthalmology & Visual Science. 2013;54(15):1029-.
37. Ahnood A, Escudie MC, Cicione R, Abeyrathne CD, Ganesan K, Fox KE, et al. Ultrananocrystalline diamond-CMOS device integration route for high acuity retinal prostheses. Biomed Microdevices. 2015;17(3).
38. Apollo NV, Lau D, Ahnood A, Stacey A, Ganesan K, Lichter SG, et al. Brazing techniques for the fabrication of biocompatible carbon-based electronic devices. Carbon. 2016;107:180-9.
39. Chan LLH, Lee EJ, Humayun MS, Weiland JD. Both electrical stimulation thresholds and SMI-32-immunoreactive retinal ganglion cell density correlate with age in S334ter line 3 rat retina. J Neurophysiol. 2011;105(6):2687-97.
40. Cho A, Ratliff C, Sampath A, Weiland J. Changes in ganglion cell physiology during retinal degeneration influence excitability by prosthetic electrodes. J Neural Eng. 2016;13(2).
41. Margolis DJ, Newkirk G, Euler T, Detwiler PB. Functional stability of retinal ganglion cells after degeneration-induced changes in synaptic input. J Neurosci. 2008;28(25):6526-36.
42. Thevenaz P, Unser M. User-friendly semiautomated assembly of accurate image mosaics in microscopy. Microscopy Research and Technique. 2007;70(2):135-46.
43. Schindelin J, Arganda-Carreras I, Frise E, Kaynig V, Longair M, Pietzsch T, et al. Fiji: an open-source platform for biological-image analysis. Nat Methods. 2012;9(7):676-82.
44. Wong RCS, Cloherty SL, Ibbotson MR, O'Brien BJ. Intrinsic physiological properties of rat retinal ganglion cells with a comparative analysis. J Neurophysiol. 2012;108(7):2008-23.
45. Chen KF, Yang Z, Hoang L, Weiland J, Humayun M, Liu WT. An Integrated 256-Channel Epiretinal Prosthesis. Ieee J Solid-St Circ. 2010;45(9):1946-56.
46. Tran N, Bai S, Yang JW, Chun H, Kavehei O, Yang YY, et al. A Complete 256-Electrode Retinal Prosthesis Chip. Ieee J Solid-St Circ. 2014;49(3):751-65.
47. Liu K, Wang Y, Yin ZQ, Weng CH. Light-Evoked Currents in Retinal Ganglion Cells from Dystrophic RCS Rats. Ophthalmic Res. 2013;50(3):141-50.
48. Ryals RC, Andrews MD, Datta S, Coyner AS, Fischer CM, Wen Y, et al. Long-term characterization of retinal degeneration in Royal College of Surgeons rats using spectral-domain optical coherence tomography. Invest Ophth Vis Sci. 2017;58(3):1378-86.
49. Jensen RJ, Rizzo JF. Activation of ganglion cells in wild-type and rd1 mouse retinas with monophasic and biphasic current pulses. J Neural Eng. 2009;6(3).
50. Sekirnjak C, Hulse C, Jepson LH, Hottowy P, Sher A, Dabrowski W, et al. Loss of responses to visual but not electrical stimulation in ganglion cells of rats with severe photoreceptor degeneration. J Neurophysiol. 2009;102(6):3260-9.
51. Suzuki S, Humayun MS, Weiland JD, Chen S-J, Margalit E, Piyathaisere DV, et al. Comparison of electrical stimulation thresholds in normal and retinal degenerated mouse retina. Japanese journal of ophthalmology. 2004;48(4):345-9.
52. Behrend MR, Ahuja AK, Humayun MS, Weiland JD, Chowe RH. Selective labeling of retinal ganglion cells with calcium indicators by retrograde loading in vitro. J Neurosci Meth. 2009;179(2):166-72.
53. Borghuis BG, Tian L, Xu Y, Nikonov SS, Vardi N, Zemelman BV, et al. Imaging Light Responses of Targeted Neuron Populations in the Rodent Retina. J Neurosci. 2011;31(8):2855-67.
54. Briggman KL, Euler T. Bulk electroporation and population calcium imaging in the adult mammalian retina. J Neurophysiol. 2011;105(5):2601-9.
55. Cameron M, Kekesi O, Morley JW, Tapson J, Breen PP, van Schaik A, et al. Calcium Imaging of AM Dyes Following Prolonged Incubation in Acute Neuronal Tissue. Plos One. 2016;11(5).
56. Weitz AC, Behrend MR, Lee NS, Klein RL, Chiodo VA, Hauswirth WW, et al. Imaging the response of the retina to electrical stimulation with genetically encoded calcium indicators. J Neurophysiol. 2013;109(7):1979-88.
57. Im M, Fried SI. Temporal properties of network-mediated responses to repetitive stimuli are dependent upon retinal ganglion cell type. J Neural Eng. 2016;13(2):025002.
58. Baden T, Berens P, Franke K, Roson MR, Bethge M, Euler T. The functional diversity of retinal ganglion cells in the mouse. Nature. 2016;529(7586):345-+.
59. Fan VH, Grosberg LE, Madugula SS, Hottowy P, Dabrowski W, Sher A, et al. Epiretinal stimulation with local returns enhances selectivity at cellular resolution. J Neural Eng. 2019;16(2).
60. Guo T, Yang CY, Tsai D, Muralidharan M, Suaning GJ, Morley JW, et al. Closed-Loop Efficient Searching of Optimal Electrical Stimulation Parameters for Preferential Excitation of Retinal Ganglion Cells. Front Neurosci-Switz. 2018;12.

61. Twyford P, Cai C, Fried S. Differential responses to high-frequency electrical stimulation in ON and OFF retinal ganglion cells. J Neural Eng. 2014;11(2).
62. Boinagrov D, Pangratz-Fuehrer S, Goetz G, Palanker D. Selectivity of direct and network-mediated stimulation of the retinal ganglion cells with epi-, sub- and intraretinal electrodes. J Neural Eng. 2014;11(2).
63. Eickenscheidt M, Jenkner M, Thewes R, Fromherz P, Zeck G. Electrical stimulation of retinal neurons in epiretinal and subretinal configuration using a multicapacitor array. J Neurophysiol. 2012;107(10):2742-55.
64. Hadjinicolaou AE, Savage CO, Apollo NV, Garrett DJ, Cloherty SL, Ibbotson MR, et al. Optimizing the Electrical Stimulation of Retinal Ganglion Cells. Ieee Transactions on Neural Systems and Rehabilitation Engineering. 2015;23(2):169-78.
65. Jensen RJ, Ziv OR, Rizzo JF. Thresholds for activation of rabbit retinal ganglion cells with relatively large, extracellular microelectrodes. Invest Ophth Vis Sci. 2005;46(4):1486-96.
66. Margalit E, Thoreson WB. Inner retinal mechanisms engaged by retinal electrical stimulation. Invest Ophth Vis Sci. 2006;47(6):2606-12.
67. Grosberg LE, Ganesan K, Goetz GA, Madugula SS, Bhaskhar N, Fan V, et al. Activation of ganglion cells and axon bundles using epiretinal electrical stimulation. J Neurophysiol. 2017;118(3):1457-71.
68. Stronks HC, Dagnelie G. The functional performance of the Argus II retinal prosthesis. Expert Rev Med Devic. 2014;11(1):23-30.
69. Bonham BH, Litvak LM. Current focusing and steering: Modeling, physiology, and psychophysics. Hearing Res. 2008;242(1-2):141-53.
70. Jones BW, Marc RE. Retinal remodeling during retinal degeneration. Exp Eye Res. 2005;81(2):123-37.
71. Apushkin MA, Fishman GA, Alexander KR, Shahidi M. Retinal thickness and visual thresholds measured in patients with retinitis pigmentosa. Retina. 2007;27(3):349-57.